Appl Phys A (2008) 93: 711–716
DOI 10.1007/s00339-008-4701-1

Applied Physics A
Materials Science & Processing

The influence of lithium excess in the target on the properties and compositions of $Li_{1+x}Mn_2O_{4-\delta}$ thin films prepared by PLD

F. Simmen · T. Lippert · P. Novák · B. Neuenschwander · M. Döbeli · M. Mallepell · A. Wokaun

Received: 12 October 2007 / Accepted: 4 March 2008 / Published online: 17 June 2008
© Springer-Verlag 2008

Abstract Li–Mn–O thin films were deposited by pulsed laser deposition (PLD) onto stainless steel substrates using targets containing different concentrations of added Li_2O. The influence of the target composition on the stoichiometry of the resulting thin films, the surface morphology and the electrochemical properties was studied. The application of the target with added 7.5 mol% Li_2O results in an almost ideal lithium content, while all films were still oxygen deficient. The thin films were applied as electrodes in $Li//Li_{1+x}Mn_2O_{4-\delta}$ cells (i.e. model cells for a rechargeable Li-ion battery) and characterized by cyclic voltammetry and galvanostatic charge/discharge experiments. The electrochemical measurements of the thin films confirmed that the thin films can serve as good model systems and that they show a sufficient cyclability.

PACS 81.15.Fg · 82.47.Aa

1 Introduction

Rechargeable lithium-ion batteries utilizing a lithium metal oxide as positive electrode are nowadays commonly used in mobile applications such as cameras, laptop computers and mobile phones. The alternative electroactive material, the spinel $LiMn_2O_4$ (space group Fd3m), has several potential advantages compared to the currently used layered $LiCoO_2$. The most important advantages of $LiMn_2O_4$ are its particularly low toxicity and lower cost, while the high capacity fading and the probability for the formation of a passive layer during cycling are the challenges [1].

$LiMn_2O_4$ can be synthesized by different methods, e.g. a soft chemistry method [2], hard-template routes [3], electrostatic spray deposition [4], solid-state reactions [5], spray pyrolysis [5], melt impregnation [6] and in the forms of thin films by pulsed laser deposition (PLD) [7–15]. The advantage of thin films as cathode materials is the possibility to study the lithium insertion process and the electrode/electrolyte interface reactions during cycling of pure $Li_xMn_2O_4$. This means that, unlike with powder-based electrodes, additives such as conductive carbon and binder materials are not present. Thin oxide films can therefore be applied as model electrodes, i.e. ideal dense two-dimensional electrodes, which are superior to porous composite electrodes, where the influence of the other materials may influence the characterization. Pulsed laser deposition has one disadvantage, consisting in the control of the composition, which is difficult for volatile light elements [9], such as lithium. These light elements are scattered by background gas molecules or other species in the plasma, or are sputtered from the growing film by energetic species arriving at the substrate surface. Pulsed laser deposition of $LiMn_2O_4$ on different substrate materials such as titanium foil [10], silicon [10, 13–15], indium tin oxide (ITO) [7], Pt [12] and stainless steel (SS) [8, 11, 14] has been reported previously, but the composition, especially the Li content, has not been analysed in detail, probably due to the difficulties of quantifying light elements.

F. Simmen · T. Lippert (✉) · P. Novák · A. Wokaun
General Energy Research Department, Paul Scherrer Institut,
5232 Villigen PSI, Switzerland
e-mail: thomas.lippert@psi.ch

B. Neuenschwander
Institut für angewandte Lasertechnologie,
Mikromaterialbearbeitung, Berner Fachhochschule,
3400 Burgdorf, Switzerland

M. Döbeli · M. Mallepell
Ion Beam Physics, Paul Scherrer Institut and ETH Zurich,
8093 Zurich, Switzerland

source: https://doi.org/10.24451/arbor.11303 | downloaded: 5.5.2023

O'Mahony et al. [16] and Dumont et al. [10] have shown that the deposition of $Li_{1+x}Mn_2O_{4-\delta}$ is not congruent, due to the above-described scattering and sputtering. Julien et al. [15] suggested to overcome the loss of lithium by applying targets with lithium excess. They used targets with different compositions by varying the addition of Li_2O from 5 to 15% in order to achieve a Li/Mn ratio >0.5. With 15% they obtained pulsed laser deposited films with the desired lithium content of 1 [15].

The oxygen deficiency in pulsed laser deposited thin $Li_{1+x}Mn_2O_{4-\delta}$ films was also studied e.g. by Dumont et al. [10] and a post-deposition treatment in oxygen atmosphere has been suggested to overcome oxygen deficiencies.

The aim of this study was to follow and to advance the approach by Julien et al. [15] to achieve a lithium content of slightly higher than 1, ideally the same as in the slightly overlithiated powder (Li/Mn = 0.515) that has been used for the target preparation. This composition has been determined to be the optimum considering both capacity and capacity fading for electrodes with powder materials [17, 18]. The PLD films were used for the thin-film studies as deposited, i.e. without further treatment to change the oxygen content.

Targets with various amounts of additional Li_2O were applied to understand the deposition process of the $Li_{1+x}Mn_2O_{4-\delta}$ (LMO) thin films on stainless steel (SS). The influence of the different amounts of added Li_2O on the chemical composition, the crystallinity, the surface morphology and the electrochemical properties was analysed in detail.

2 Experimental

2.1 Film preparation

Thin films of $Li_{1+x}Mn_2O_{4-\delta}$ were prepared by PLD (pulsed laser deposition) using a KrF excimer laser (Lambda Physik, 248 nm, 20 ns, 10 Hz, 4.0–4.3 J cm^{-2}). Stainless steel was used as substrate material at a deposition temperature of ~500°C using a silicon wafer for resistance heating. The substrate–target distance was fixed at 4 cm. The deposition was performed with an oxygen background pressure of 0.2 mbar with 18000 pulses. After deposition the thin films were cooled in the oxygen background pressure of 0.2 mbar within 30 min to ~30°C.

Different target compositions ($Li_{1.03}Mn_2O_4 + xLi_2O$, $x = 0, 2.5, 7.5, 12.5$ mol%) were used. The targets ($Li_{1.03}Mn_2O_4 + xLi_2O$) were prepared by mixing $Li_{1.03}Mn_2O_4$ (99.7% purity, Honeywell, Li/Mn = 0.515) and Li_2O (99.5% purity, Alfa Aesar) powders, then pressing a rod with 4000 bar ($x = 2.5$, 7.5, 12.5 mol%) or 2000 bar ($x = 0$ mol%), respectively, and finally sintering the obtained rods at 750°C in oxygen for 10 h ($x = 2.5$, 7.5, 12.5 mol%) or 24 h ($x = 0$ mol%).

The stoichiometry of the thin films was measured by combining Rutherford backscattering spectrometry (RBS) with elastic recoil detection analysis (ERDA). RBS is generally slightly more accurate than ERDA, but Li cannot reasonably be detected by this technique. Therefore, only the O/Mn ratio was determined by RBS while the Li/O ratio was obtained from ERDA measurements with iodine projectiles using $LiNbO_3$ material as a standard. The crystallinity was measured with X-ray diffractometry (XRD, Siemens D-500 X-ray diffractometer, 0.014° step size, time per step: 2 s, range: 12–85°, Ni filter). The surface was characterized with scanning electron microscopy (SEM, in-lens detector, 1 kV/12 kV at 10^{-5} mbar) and atomic force microscopy (AFM, contact mode). The film thickness was measured by profilometry (Dektak 8).

2.2 Electrochemical characterization

The test cell consisted of a thin oxide film as positive electrode and a metallic Li foil (Aldrich) as negative electrode, which was also used as a reference electrode. The electrodes were separated with a glass fibre separator, while a solution of 1 M $LiPF_6$ (Ferro) in 1:1 EC:DMC (LP30 Ferro, EC: ethylene carbonate, DMC: dimethyl carbonate) was used as electrolyte. The thin films were cycled in the potential range of 3.5–4.4 V vs. Li/Li$^+$. The cell assembly was performed in an argon-filled glove box (content of H_2O of <0.1 ppm, O_2 of ~0.6 ppm). After cycling, the thin-film electrodes were washed with DMC, dried in vacuum at 80°C for 10 min, and used for post-mortem characterization.

The thin films were electrochemically analysed after the characterization in half cells by cyclic voltammetry at 0.05 mV s^{-1} for 20 cycles between 3.5 V and 4.4 V vs. Li/Li$^+$ and then a galvanostatic charge/discharge (1 C rate, 1 C ≅ 13 μA cm^{-2}) experiment, finally followed by cyclic voltammetry (0.05 mV s^{-1}, 20 cycles, 3.5–4.4 V vs. Li/Li$^+$). The irreversible capacity Q_{irr} (shown in Fig. 5) was calculated as $Q_{irr} = (Q_C - Q_D)/Q_C$, where Q_C and Q_D are the charge (Li$^+$ extraction) and discharge (Li$^+$ insertion) capacities, respectively.

3 Results and discussion

3.1 Film characterization: crystallinity, surface morphology and composition

Figure 1 shows the XRD pattern of the prepared thin polycrystalline films. The thin films on stainless steel have, as expected, no preferred growth orientation. The marked reflexes

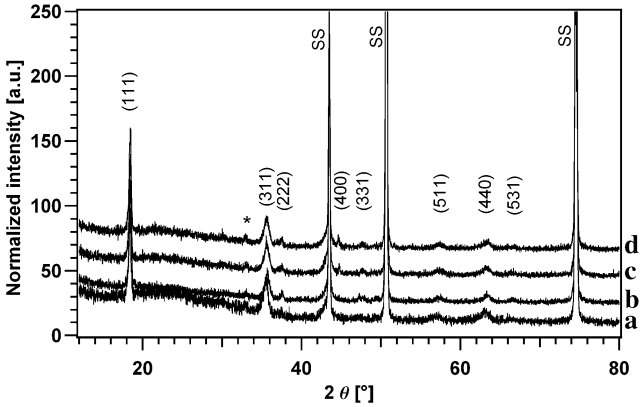

Fig. 1 XRD patterns of $Li_{1+x}Mn_{2-y}O_{4-\delta}$ thin films deposited by PLD with targets of different compositions ($Li_{1.03}Mn_2O_4 + xLi_2O$; x =(**a**) 0, (**b**) 2.5, (**c**) 7.5, (**d**) 12.5 mol%) (SS = stainless steel, * = Mn_2O_3)

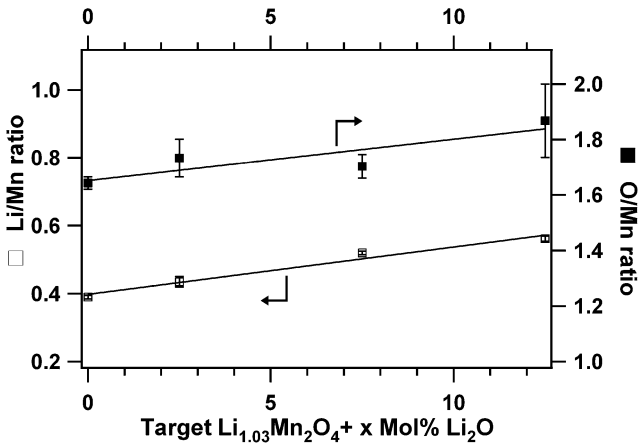

Fig. 2 Li/Mn and O/Mn ratios as function of the target composition ($Li_{1.03}Mn_2O_4 + xLi_2O$; $x = 0$, 2.5, 7.5, 12.5 mol%)

(*hkl*) (see Fig. 1) can be assigned to the $LiMn_2O_4$ cubic spinel structure. The other reflexes, which are marked with SS, correspond to the substrate, i.e. stainless steel. The weak reflex around 32.9°(marked by an *) is probably Mn_2O_3. The loss of the volatile lithium during film deposition may be the reason for the secondary phase (Mn_2O_3) and/or the cause of lithium sub-stoichiometrical compositions.

The compositions of the thin films, which were determined with RBS and ERDA measurements, are summarized in Fig. 2. Both the O/Mn ratio and the Li/Mn ratio are increasing with increasing lithium content in the target. The increasing O/Mn ratio is due to the increasing oxygen content in the target with increasing concentration of Li_2O. The oxygen content of the Li-spinel is still below the stoichiometric content of 4 and probably results in the formation of oxygen vacancies. The increase of the oxygen and lithium contents in the thin films is almost linear with increasing concentrations of Li_2O in the target. The target with 7.5 mol% of added Li_2O results in films with the desired lithium content of approx. 1.04. The loss of lithium, comparing the target and the film compositions, is decreasing from 24.3 to 11.7% with increasing lithium content in the target. This could be due to a higher probability for lithium to reach the substrate without collisions. Depth profiles, i.e. the distribution of the elements through the film thickness, were determined by ERDA measurements and confirm a homogeneous distribution of lithium, manganese and oxygen through the film.

The calculated compositions of the films, depending on the target composition ($Li_{1.03}Mn_2O_4 + xLi_2O$), are: $Li_{0.78}Mn_2O_{3.29}$ ($x = 0$ mol%), $Li_{0.87}Mn_2O_{3.47}$ ($x =$ 2.5 mol%), $Li_{1.04}Mn_2O_{3.41}$ ($x = 7.5$ mol%) and $Li_{1.13}Mn_2O_{3.73}$ ($x = 12.5$ mol%). The analytical results are normalized to the manganese content of 2.

The surface morphology of the films, which was obtained by AFM measurements, reveals particles (grains) with a diameter of 0.3–0.5 µm. The number and packaging of the small particles seem to decrease with increasing lithium contents of the target and of the film. The RMS (root mean square) roughness of the thin films is increasing slightly with increasing Li_2O content in the target (from 20 to 35 nm), which correlates well with the SEM analyses (see Fig. 3a–d). Particles with flake and plate shapes (Fig. 3a, c, d) as well as particles with a rod-like (Fig. 3b) appearance are visible.

The thickness of the films increases with increasing lithium excess, i.e. from 230 to 300 nm. This may be due to the increasing film roughness, lower density of the particles and/or from an increase of the ablation rates with increasing lithium excess in the target (due to the higher laser penetration depth).

3.2 Electrochemical characterization of the thin films

The electrochemical properties of the thin films were studied with cyclic voltammetry (CV) and galvanostatic charge/discharge experiments. The measured cyclic voltammograms (see Fig. 4) show the characteristic two redox peak pairs of $LiMn_2O_4$, corresponding to the two oxidation (in the range of about 4.01/4.14 V vs. Li/Li^+) and two reduction steps (in the range of about 3.99/4.12 V). In the first oxidation step half of the lithium is extracted theoretically and $Li_{0.5}Mn_2O_4$ is formed. In the second step the rest of the residual lithium is removed and λ-MnO_2 is formed [7, 19], as described by the following chemical equations:

$$LiMn_2O_4 \longrightarrow (1/2)\ Li^+ + (1/2)\ e^- + Li_{0.5}Mn_2O_4,$$
$$Li_{0.5}Mn_2O_4 \longrightarrow (1/2)\ Li^+ + (1/2)\ e^- + 2\ \lambda\text{-}MnO_2$$

The observed peak positions of lithium insertion and deinsertion match well with those for the powder material [20]. After 120 cycles the normalized current density is decreasing, which is most probably due to degradation of the films

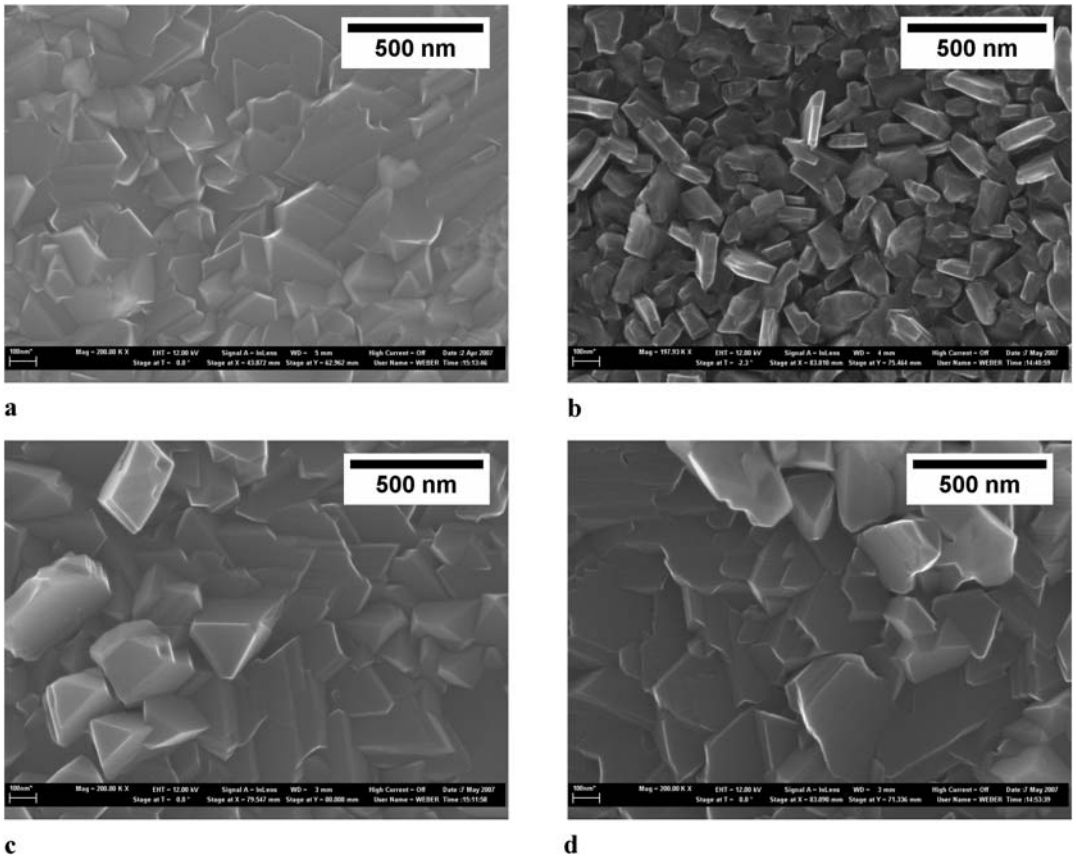

Fig. 3 SEM images of films with different lithium and oxygen contents: (**a**) $Li_{0.78}Mn_2O_{3.29}$, (**b**) $Li_{0.87}Mn_2O_{3.47}$, (**c**) $Li_{1.04}Mn_2O_{3.41}$, (**d**) $Li_{1.13}Mn_2O_{3.73}$

Table 1 Charge and discharge capacities after two and 10 cycles of the thin films. The capacities have been normalized to the film thickness

Sample	Normalized charge capacity Q_C [μA h cm^{-2} μm^{-1}] (±10%)		Normalized discharge capacity Q_D [μA h cm^{-2} μm^{-1}] (±10%)	
	$Q_{C,2}$	$Q_{C,10}$	$Q_{D,2}$	$Q_{D,10}$
$Li_{0.78}Mn_2O_{3.29}$	55	49	39	36
$Li_{0.87}Mn_2O_{3.47}$	37	33	42	40
$Li_{1.04}Mn_2O_{3.41}$	39	34	32	30
$Li_{1.13}Mn_2O_{3.73}$	31	28	33	30

during cycling. A significant shift of the redox peaks with the cycle number is not observed, suggesting that the insertion and deinsertion mechanism does not change.

In Table 1 the data derived from the electrochemical analysis are summarized. For the second galvanostatic cycle the obtained range was 31–55 μA h cm^{-2} μm^{-1} (±10%) for the normalized charge capacity and 32–42 μA h cm^{-2} (±10%) for the normalized discharge capacity, respectively. The highest normalized charge capacity is observed for $Li_{0.78}Mn_2O_{3.29}$. It is noteworthy to mention that impurities, if present, could influence the charge and discharge capacities of the thin films (cf. Fig. 1, where an additional weak reflex marked by * is observed, possibly from Mn_2O_3).

Galvanostatic cycling with various charge/discharge rates up to 16 C (assuming 1 C ≅ 13 μA cm^{-2}) showed for all thin films a good cyclability (Fig. 5), because after 100 deep cycles the thin films showed a retained capacity >60%. The retained capacity (in %) is defined as $C_x/C_2 \times 100$ (C_2 = charge capacity after two cycles, C_x = charge capacity after x cycles). The influence of the different film stoichiometries is visible in the retained capacities for different charge rates for the thin film. The specific charge and discharge capacities, and the irreversible capacity of the thin film with the best cycling stability ($Li_{1.13}Mn_2O_{3.73}$), are shown in Fig. 5 (bottom). The negative irreversible capacity is due to the slightly higher reduction (discharge) than oxidation (charge) in the respective cycle.

4 Conclusion

The present work confirms that the preparation of polycrystalline thin Li–Mn–O films with a desired lithium content

is possible by pulsed laser deposition. The lithium loss during the deposition process decreases with increasing lithium content in the target from 24.3 to 11.7%. The target with a composition of $Li_{1.03}Mn_2O_4 + 7.5$ mol% Li_2O yielded films with the desired Li/Mn ratio of about 1.04. A Mn_2O_3 impurity was detected in some thin films, which could explain their observed lower charge capacity. All prepared thin films exhibit a good electrochemical cycle stability, confirming their applicability for detailed studies of the lithium insertion/deinsertion processes. In the cyclic voltammograms

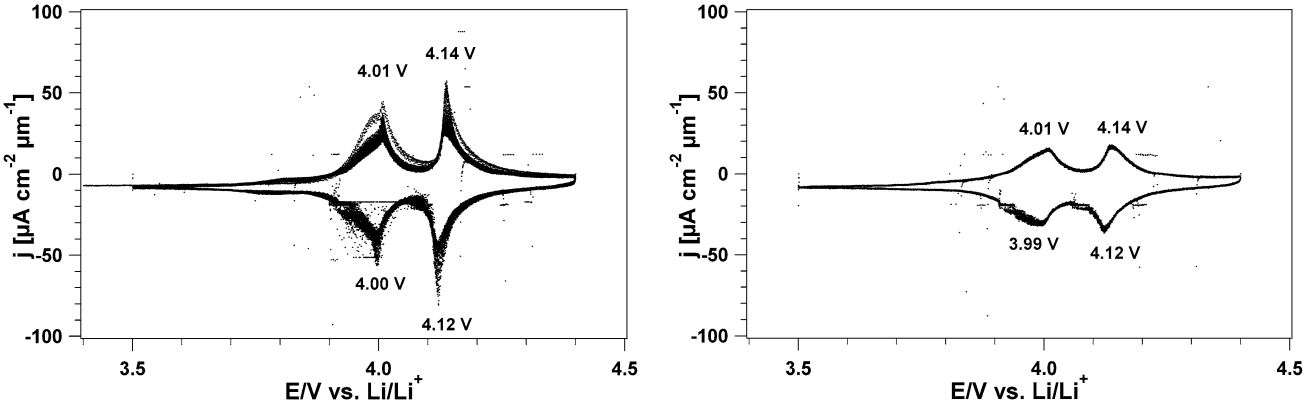

Fig. 4 Typical cyclic voltammograms at 0.05 mV s^{-1} of thin films of $Li_{0.87}Mn_2O_{3.47}$ after 20 (*left*) and 140 (*right*) cycles; 20 cycles are shown

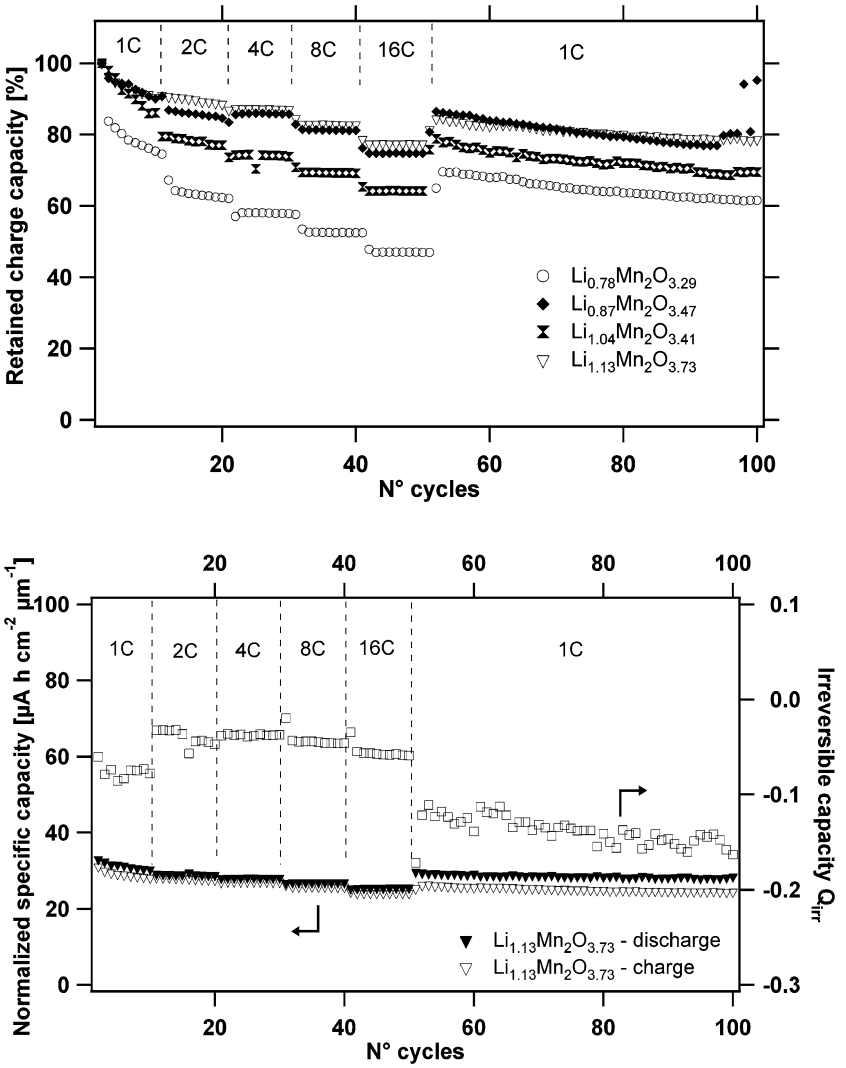

Fig. 5 (*top*) Charge capacities of the thin films for different C rates; (*bottom*) specific charge and discharge capacities, and the irreversible capacity of the $Li_{1.13}Mn_2O_{3.73}$ film. The capacities have been normalized to the film thickness

the observed peak positions of lithium insertion and deinsertion matched well with these obtained from conventional porous electrodes containing $LiMn_2O_4$.

Acknowledgements We wish to thank Anja Weber (Laboratory for Micro- and Nanotechnology, PSI Villigen, Switzerland) for the SEM measurements and the members of the Materials and Batteries Groups for their support. Furthermore, we wish to thank the Swiss National Science Foundation, the Paul Scherrer Institut and the ESF (DYNA program) for financial support.

References

1. S.R. Das, I.R. Fachini, S.B. Majumder, R.S. Katiyar, J. Power Sources **158**, 518 (2006)
2. K. Suryakala, K.R. Marikkannu, G.P. Kalaignan, T. Vasudevan, Ionics **13**, 41 (2007)
3. J. Cabana, T. Valdes-Solis, M.R. Palacin, J. Oro-Sole, A. Fuertes, G. Marban, A.B. Fuertes, J. Power Sources **166**, 492 (2007)
4. D. Shu, K.Y. Chung, W.I. Cho, K.-B. Kim, J. Power Sources **114**, 253 (2003)
5. D.Y.K. Seo Hee Ju, E.B. Jo, Y.C. Kang, J. Ceram. Soc. Jpn. **115**, 241 (2007)
6. Y. Xia, M. Yoshio, J. Power Sources **66**, 129 (1997)
7. H. Otsuji, K. Kawahara, T. Ikegami, K. Ebihara, Thin Solid Films **506–507**, 120 (2006)
8. A. Rougier, K.A. Striebel, S.J. Wen, T.J. Richardson, R.P. Reade, E.J. Cairns, Appl. Surf. Sci. **134**, 107 (1998)
9. C. Ouyang, H. Deng, Z. Ye, M. Lei, L. Chen, Thin Solid Films **503**, 268 (2006)
10. T. Dumont, T. Lippert, M. Dobeli, H. Grimmer, J. Ufheil, P. Novak, A. Wursig, U. Vogt, A. Wokaun, Appl. Surf. Sci. **252**, 4902 (2006)
11. A. Rougier, K.A. Striebel, S.J. Wen, E.J. Cairns, J. Electrochem. Soc. **145**, 2975 (1998)
12. D. Singh, R. Houriet, R. Giovannini, H. Hofmann, V. Craciun, R.K. Singh, J. Power Sources **97–98**, 826 (2001)
13. M.A. Camacho-Lopez, L. Escobar-Alarcon, E. Haro-Poniatowski, C. Julien, Ionics **5**, 244 (1999)
14. S.B. Tang, M.O. Lai, L. Lu, S. Tripathy, J. Solid State Chem. **179**, 3831 (2006)
15. C. Julien, E. Haro-Poniatowski, M.A. Camacho-Lopez, L. Escobar-Alarcon, J. Jimenez-Jarquin, Mater. Sci. Eng. B **72**, 36 (2000)
16. D. O'Mahony, J. Lunney, T. Dumont, S. Canulescu, T. Lippert, A. Wokaun, Appl. Surf. Sci. **254**, 811 (2007)
17. D. Guyomard, J.M. Tarascon, Solid State Ionics **69**, 222 (1994)
18. Y.-K. Sun, Solid State Ionics **100**, 115 (1997)
19. M. Morcrette, P. Barboux, J. Perriere, T. Brousse, A. Traverse, J.P. Boilot, Solid State Ionics **138**, 213 (2001)
20. S.S. Zhang, T.R. Jow, J. Power Sources **109**, 172 (2002)